University of Reading

Revisiting the interaction between Antarctic Sea ice and Southern Ocean cyclones

Article

Accepted Version

Zhong, R., Hodges, K. ORCID: https://orcid.org/0000-0003-0894-229X, Yang, Q. and Chen, D. (2025) Revisiting the interaction between Antarctic Sea ice and Southern Ocean cyclones. Journal of Geophysical Research, 130 (8). e2024JD042914. ISSN 2156-2202 doi: 10.1029/2024JD042914 Available at https://centaur.reading.ac.uk/122379/

It is advisable to refer to the publisher's version if you intend to cite from the work. See Guidance on citing.

To link to this article DOI: http://dx.doi.org/10.1029/2024JD042914

Publisher: American Geophysical Union

All outputs in CentAUR are protected by Intellectual Property Rights law, including copyright law. Copyright and IPR is retained by the creators or other copyright holders. Terms and conditions for use of this material are defined in the End User Agreement.

www.reading.ac.uk/centaur

University of Reading

CentAUR

Central Archive at the University of Reading

Reading's research outputs online

Revisiting the Interaction Between Antarctic Sea Ice and Southern Ocean Cyclones

Rui Zhong[1], Kevin Hodges[2], Qinghua Yang[1*], and Dake Chen[1]

[1] School of Atmospheric Science, Sun Yat-sen University, and Southern Marine Science and Engineering Guangdong Laboratory (Zhuhai), Zhuhai, China.

[2] National Centre for Atmospheric Science (NCAS) and Department of Meteorology, University of Reading, Reading, United Kingdom.

Corresponding author: Qinghua Yang (yangqh25@mail.sysu.edu.cn)

Key Points:

- There is an inconsistent seasonal shift between storm track and sea ice edge.
- The high exposure areas of sea ice to cyclones are concentrated at the edges.
- Short-term sea ice responses various depends on the path and strength of cyclones.

Abstract

The sea ice around Antarctica undergoes a natural seasonal cycle of slow advance and rapid retreat, which does not align with the seasonal north-south shift of the storm track over the Southern Ocean. In particular, cyclones near the sea ice edge have a stronger impact on the sea ice compared to those occurring elsewhere across the Southern Ocean. Despite the increasing long-term trend of sea ice reversing after 2015, further investigation shows a significant increase in the number of ice-linked cyclones in almost all subregions. To better understand the seasonal and regional relationship between sea ice and cyclones, an exposure index is introduced, encompassing various features of cyclones, local sea ice concentration (SIC), and their interaction time. This index helps identify key seasons for each subregion. Analyzing cyclones categorized by local SIC anomaly, we observe that cyclone strength and movement direction significantly influence SIC anomalies. Composite results highlight the critical role of temperature advection and surface sensible heat flux in SIC changes driven by cyclone circulation. Though these results depend on the cyclone's interaction with the background circulation and its position relative to the sea ice edge, they offer a new perspective on short-term sea ice changes from a cyclone perspective and improve the representation of cyclone-sea ice interactions in climate models, enhancing predictions of future Antarctic sea ice trends.

Plain Language Summary

As storm tracks in the Southern Ocean shift poleward due to climate change, more cyclones are expected to impact Antarctic sea ice. This study specifically examines Southern Ocean cyclones that affect sea ice, revealing that seasonal and regional differences in cyclone characteristics shape the relationship between cyclones and sea ice. Composite results indicate that variations in cyclone intensity and movement direction relative to the sea ice edge can produce four distinct responses in local sea ice concentration, driven by the cyclonic wind field and associated warm or cold air. This suggests that the short-term impacts of passing cyclones on sea ice are not singular.

1 Introduction

Antarctic sea ice exhibits one of the largest seasonal signals on Earth, with significant implications for the planetary albedo, energy exchange between the atmosphere and ocean, thermohaline circulation, and ocean productivity (Eayrs et al., 2019, 2021; Clem et al., 2022). In contrast to the consistent decrease in Arctic sea ice since 1978 (Serreze & Stroeve, 2015), Antarctic sea ice has shown greater variability, with a dramatic trend reversal from growth to decline since 2014 (Turner et al., 2017; Parkinson & DiGirolamo, 2016; 2021), and characterized by strong regional and seasonal differences over the long term (Parkinson 2019; Eayrs et al., 2021; Pirti et al., 2022). Current research has tried to understand these long-term and asymmetric changes in Antarctic sea ice from both atmospheric and oceanic perspectives (Meehl et al., 2019). However, there is still no consensus in explaining these observed changes (Hobbs et al., 2016; Jones et al., 2016; Parkinson & DiGirolamo, 2021).

An increasing number of record low sea ice events have been observed in both hemispheres since 2010, and extratropical cyclones have been considered to play an important role in these events. In the Arctic, the 2012 record low Arctic sea ice cover was attributed to a strong storm that entered the central Arctic in early August (Simmonds & Rudeva 2012). Additionally, two August storms contributed to another record low in the Arctic in 2016 (Petty et al., 2018). Strong storms can separate a small portion of the sea ice from the main ice pack and cause further decay in the main pack by increasing its exposure to wind and waves (Parkinson & Comiso 2013). The storm-induced enhanced oceanic mixing can also lead to bottom melt and a significant decrease in ice volume (Zhang & Lindsay 2013). Similarly, in the Antarctic, strong cyclones drove unprecedented ice loss in the Weddell Sea during the austral spring and summer of 2016/17 by advecting multi-year ice northward into warmer and lower latitudes (Turner et al., 2020). A few months later, strong cyclones further triggered the re-occurrence of the Maud Rise Polynya in the 2017 austral winter (Francis et al., 2019). The large negative anomaly of sea ice extent (SIE) in the Weddell Sea during April and May 2019 was caused by a series of intense and explosive polar cyclones (Jena et al., 2022a). Record low sea ice events in other regions of Antarctica have also been found to be linked to cyclone activity. For instance, a series of intense polar cyclones in late 2021 resulted in a strong offshore flow and coastal polynya in the Ross Sea, accelerating sea ice loss through increased solar radiation absorption and nonlinear ice-albedo feedback, resulting in a record low in February 2022 (Turner et al., 2022; Wang et al., 2022). In the extreme sea ice loss of 2023, cyclones intensified northerly winds and subsequently caused a significant retreat in the Weddell Sea and Ross Sea (Jena et al., 2024). Although there is a different land-sea distribution and more variable sea ice trends in the Southern Hemisphere compared to that in the Northern Hemisphere, it appears that cyclones may play a crucial role in modulating the SIE in the Southern Hemisphere as well.

High-latitude cyclones act as a bridge connecting hemisphere-wide climate variability and sea ice in many complex ways (Yuan et al., 1999; Vihma 2014). Specifically, in low sea ice concentration regions, the transfer of high amounts of latent and sensible heat to the atmosphere would be expected to increase baroclinicity and promote the development of atmospheric disturbances (Watkins & Simmonds, 1995). Thus, a decrease in SIE may increase the number of cyclones (Simmonds & Wu 1993), which, in turn, could drive a southward shift of high-latitude cyclones and potentially enhance downstream cyclone density (Pezza et al., 2008). Although some studies suggest that atmospheric stresses and the topographic asymmetry of the Antarctic continent (Howarth 1983; Godfred-Spenning & Simmonds 1996), instead of sea ice, dominate the density and track of cyclones, less sea ice accompanied by changes in cold air outbreaks and baroclinic properties do affect the storm track and cyclogenesis (Menéndez et al., 1999; Yuan et al., 1999). On the other hand, strong winds related to cyclone systems may alter the distribution of sea ice through advection and their impact of surface stress on the ice surface (Watkins & Simmonds 1998), affecting the speed at which water in them refreezes (Dare & Atkinson, 1999), roughing the older sea ice in the frontal ice zone (Nghiem et al., 2016) and inducing a rapid growth of sea ice in specific regions (Wang et al., 2014). In addition to the effect of wind, the cyclone-induced dynamic (poleward propagation of ocean waves and ice motion) and thermodynamic (heat and moisture plumes from midlatitudes, ocean mixed layer warming) processes can facilitate sea ice loss (Jena et al., 2022b). Hence, cyclones influence sea ice advance

and retreat differently across seasons (Finocchio et al., 2022). Even within a single season, Mundi and L'Ecuyer (2024) observed that the increased frequency of early summer storms, which drive greater ice loss, has resulted in a more pronounced decline in the MIZ ice area compared to the 1980s. Furthermore, their findings indicate that southerly wind-enhancing summer storms in the Arctic typically reduce ice area, whereas northerly storms tend to increase it. In addition to their significant impact on the marginal ice zone (Finocchio et al., 2020; Vichi et al., 2019), cyclones contribute to polynya formation through atmospheric and oceanic processes (Francis et al., 2020; Jena et al., 2024) and influence sea ice production within polynyas (Wang et al., 2021; 2023).

Variability in Antarctic sea ice and cyclones have been linked in previous studies (Carleton 1983; Howarth 1983; Streten 1983). The correlation between sea ice and cyclones varies in different regions and over time (Carleton 1983; Howarth 1983). On an interannual timescale, positive sea ice anomalies and cold air outbreaks are closely associated with the occurrence of cyclones (Carleton & Carpenter 1989). The development and maintenance of sea ice anomalies have also been found to be significantly affected by the track, intensity, and frequency of cyclones (Streten 1983). However, due to the limited availability of observational records, conclusions of these earlier studies may only apply to specific periods and lack general applicability. Benefiting from the development and application of cyclone tracking algorithms, Simmonds and Wu (1993) found that less Antarctic sea ice leads to lower sea-level pressure as a result of more cyclones but not necessarily more intense ones. The relationship between Antarctic sea ice and Southern Ocean cyclones is regionally dependent, and not consistent across the entire sea-ice zone on a seasonal time scale (Godfred-Spenning & Simmonds 1996). Their correlation is more significant near the sea ice edge (Simmonds 2003). Local cyclone density appears more closely linked to sea ice upstream or downstream, indicating the crucial role of the 10-m wind associated with the synoptic system in the sea ice variability (Schemm 2018). In addition, the relationship also depends on the spatial and temporal scale. There are weak correlations on interannual timescales but the correlations become strong when sea ice lags both track density and cyclogenesis by one season (Godfred-Spenning & Simmonds 1996; Simmonds 1996). Zhang et al. (2023) found that this lag time is 1-2 months in austral summer using the lagged maximum covariance analysis (MCA). The above studies focus on the correlation between cyclone density and sea ice extent on different timescales and regions, but most of them barely achieve statistical significance. They also lack a reasonable explanation for the significant correlation and it is still a puzzle about the significant correlations only occur in particular seasons and regions. Cyclones with different paths and genesis locations exhibit varying meridional moisture and momentum fluxes (Sinclair & Dacre 2019; Ward et al., 2023), causing vary impacts on sea ice. Such details are hidden within the cyclone track density and result in producing a weak correlation between sea ice and cyclones. Recent findings reveal that 30-40% of extreme sea ice variability events on synoptic timescales are linked to Southern Ocean cyclones, with the characteristics of these cyclones playing a significant role in shaping their relationships in different regions (Hepworth et al., 2024).

Although there is a tug of war in the shift of the westerly jet stream in the Southern Hemisphere due to the ozone-hole recovery and increasing greenhouse gases (Perlwitz 2011), a confirmed poleward shift of the storm track can be seen in the Southern Hemisphere both in the historical record (Bender et al., 2012) and in future simulations (Tamarin-Brodsky & Kaspi 2017;

Priestley & Catto 2021). More cyclones moving closer to the Antarctic continent are likely to intensify their impact on sea ice distribution and variability. In this context, focusing on ice-linked cyclones (near or over the sea ice) will be crucial for understanding their role in shaping future sea ice dynamics. At present, we have access to comprehensive and reliable data for the Antarctic sea ice edge and sea ice concentration since 1979 from passive microwave satellites and high-resolution reanalysis data, as well as datasets of Southern Ocean cyclone tracks produced by applying objective tracking algorithms to reanalysis data. The aim of this paper is to provide a clearer picture of the interaction of cyclones with sea ice through addressing the following questions:

(1) What are the characteristics and trends of ice-linked cyclones?

(2) What is the mechanisms for the different responses of SIC to cyclones?

The paper continues as follows: Section 2 describes the reanalysis data, sea ice data, cyclone tracking method, and a sea ice exposure index used in this study. The climatology of ice-linked cyclones and the composite results for different types of cyclones are presented in Section 3. Discussion and conclusions are provided in Sections 4 and 5.

2 Data and Methods

2.1 Sea ice and reanalysis data

We use atmospheric and oceanic data from the European Centre for Medium-Range Weather Forecasts (ECMWF) fifth-generation reanalysis data (ERA5, Hersbach et al., 2020), including sea ice concentration (SIC), mean sea level pressure (MSLP), and relative vorticity at 850 hPa (VORT850). The ERA5 reanalysis data have an original spectral resolution of triangular truncation 639 (T639, ~31 km horizontal resolution) and 137 hybrid sigma vertical levels. The data are available at a 0.25-degree horizontal resolution and hourly temporal resolution since 1940. In this study, we specifically analyze the data starting from 1980 to align with the sea ice data from satellite observations. The European Organization for the Exploitation of Meteorological Satellites (EUMETSAT) Ocean and Sea Ice Satellite Application Facility (OSI SAF) reanalysis product (v409a; Eastwood et al., 2014), various versions of the HadISST2 sea ice product (Titchner & Rayner, 2014) and the operational OSI SAF product that is also part of the OSTIA product were considered for the SIC data of ERA5 (Hirahara et al., 2016; Hersbach et al., 2020), which have been widely used in previous studies (Aue et al., 2022; Jenkins et al., 2022; Hepworth et al., 2024). It should be noted that the hourly SIC data from ERA5 are updated daily but stored at hourly frequency to align with the atmospheric data.

The sea ice edge is often defined as the outermost boundary separating the open ocean and sea ice, represented by the 15% SIC contour (Goessling et al., 2016; Zampieri et al., 2019). However, its precise location can be influenced by factors such as islands in the Southern Ocean, polynyas, and semi-enclosed open water. Therefore, to address these challenges, we define a conservative sea ice edge by extending it southward by more than 0.5° latitude from the 15% SIC contour line. To better capture the north-south variability of the sea ice edge, we introduce the latitude of the ice edge (IEL) as a metric to represent its position. Subsequently, we calculate the

183 average latitude of hourly sea ice edge to obtain daily, monthly, seasonal, and yearly sea ice edge
184 positions. Additionally, the corresponding variance is computed to quantify its interannual
185 variability. Considering the trend reversal observed around 2015, we further calculate the
186 regional IEL trends for two distinct periods, 1980-2015 and 1980-2022, following the
187 methodology proposed by Maksym (2019).

188

189 2.2 Cyclone tracking

190 Using the 850 hPa relative vorticity data from ERA5 reanalysis, we track the Southern
191 Ocean cyclones from 1980 to 2022 using the objective tracking algorithm TRACK (Hodges 1994,
192 1995, 1999). To better leverage ERA5's high temporal resolution for cyclone tracking, we selected
193 a temporal resolution of 1 hour and the spatial resolution of T42 (~310 km at the equator) after
194 evaluating alternative spatial-temporal schemes (Zhong et al., 2022). The tracking process
195 consists of three steps: spectral filtering to reduce noise in the vorticity field and to focus on
196 synoptic scale cyclones, cyclone center positioning by finding the off-grid vorticity minima, and
197 optimal track construction by minimizing a cost function for track smoothness constructed from
198 changes in direction and speed subject to adaptive constraints. Tracks are filtered post-tracking
199 to retain cyclone tracks with a minimum lifespan of 2 days and a movement distance of over 1000
200 km. These criteria effectively exclude short-lived or unrealistic systems (Uotila et al., 2011). Full
201 details of the tracking are given in Zhong et al. (2022). The higher temporal resolution enables
202 accurate identification of the cyclones' initial and final track points, particularly useful for locating
203 the cyclone center over the sea ice, determining the speed and moving direction of cyclones, and
204 measuring the interaction time between the cyclone and sea ice. The spectral filtering of T42 will
205 exclude small-scale and mesoscale cyclones that have a different climatological distribution from
206 the synoptic-scale cyclones (Stoll 2022).

207 In addition, the full-resolution MSLP minima is added to the vorticity tracks and used as
208 the reference of the intensity of the cyclones. TRACK achieves this by searching for the nearest
209 minima within a 5° radius (geodesic) of the vorticity center. If a true MSLP minimum cannot be
210 found (such as open cyclones that has no closed isobaric line), the MSLP value at the location of
211 vorticity center is taken. A similar method can be used to search for the maximum SIC for each
212 track point within a 5° radius, which facilitates the distinction between ice-linked and non-ice-
213 linked track points

214 The axis of the storm track refers to the maximum track density of Southern Ocean
215 cyclones. The latitude of this axis will be used to calculate the relative distance with sea ice edge.
216 Specifically, we also defined the number of track points within a 500 km radius (Haversine
217 distance) at each grid point as the feature density, highlighting the areas of most frequent cyclone
218 activity. It is note that feature density is different from track density because track points are
219 counted on multiple grid points in feature density but once in track density.

220 The Southern Ocean is divided into five subregions (Ionita et al., 2018; Turner et al., 2017):
221 Indian Ocean (IO: 20°E-90°E), Western Pacific Ocean (WPO: 90°E-160°E), Ross Sea (RS: 160°E-
222 130°W), Amundsen-Bellingshausen Sea (ABS: 130°W-60°W), and Weddell Sea (WS: 60°W-20°E).
223 We further categorize the track points into two groups based on their relative distance from the

sea ice edge. The "inside" group comprises track points located within (south of) the sea ice edge, over the sea ice but not on land. The “outside” group contains track points located outside (north of) the sea ice edge, but with a relative distance of less than 5° of latitude to the ice edge. They will be called inside cyclones and outside cyclones respectively in the rest of the paper. This approach excludes cyclones that are distant from the sea ice and allows an analysis of the differences in the behavior of cyclones inside and outside the ice edge, as well as their respective impacts on the sea ice. It provides a possible to investigate the differences in the number and characteristics of cyclones arriving at the sea ice edge and entering the interior of the sea ice edge, offering a more detailed understanding of cyclones in the ice zone. The choice of 5° is based on findings by Simmonds (1996), who observed significant correlations between sea ice and cyclone density within relatively short distances. Here, 5° is a typical mean radius of extratropical cyclones although some cyclones may have longer fronts.

Cyclone-centered composites are performed on the re-gridded field to avoid the effects of meridional convergence in polar regions. The compositing domain extends 20° in all four cardinal directions, centered on the cyclone's vorticity center at 850hPa level. This rectangular domain is initially defined at the equator and then rotated to the cyclone center using a rotation matrix to maintain a fixed aspect ratio in meridional and zonal directions. Then, the factors fields are interpolated onto the grid using B-spline interpolation. Using a domain based on geographic coordinates makes it easier to identify direction and relative distance than a circular polar coordinate composite or a distance–azimuth radial domain used in other studies (Rudeva and Gulev 2011; Catto 2018; Ponce de León and Bettencourt 2021; Clancy et al., 2022). In particular, there is a land mask for the temperature advection at 10m level, reducing noise in the composite field. To minimize interference from upstream and downstream cyclones in the composite results, this study selects only isolated cyclones for analysis. An isolated cyclone is defined as one with no other cyclones present within 20° to the east or west.

2.3 Exposure index

The impact of cyclones on sea ice is significant and depends on its concentration. Regions with lower SIC, such as the marginal ice zone, are more significantly affected than those with higher concentrations. The number, intensity, and relative distance of passing cyclones all influence the underlying sea ice to different degrees. To comprehensively assess the impact of cyclone activity on sea ice, we have developed an exposure index for each grid point (x, y) at time t is calculated as:

$$Exposure(x,y,t) = \frac{1}{SIC(x,y,t)} \sum_{t-24}^{t+24} \sum_{n=1}^{n=m} \frac{Nor_Strength(t)}{Nor_Distance(t)+\varepsilon},$$

where $\varepsilon = 10^{-4}$ is used to avoid division by zero. m represents the total number of track points within a 5° radius of the sea ice grid point over a 2-day period.

$$Nor_Strength(t) = \frac{Strength_{case(t)} - Strength_{min}}{Strength_{max} - Strength_{min}},$$

where $Nor_Strength(t)$ is the normalized intensity (MSLP) of the cyclones, with a min-max normalized to a range of 0~1.

Since higher intensity corresponds to a greater value, we take a negative value for the mslp value at the center of the cyclone. $Strength_{case(t)}$ is the strength of cyclones at each timestep. $Strength_{max}$ and $Strength_{min}$ are the maximum and minimum strength of cyclones in the dataset, respectively.

The relative distance between the sea ice grid point and the cyclone center is denoted by a $Distance(t)$, normalized by a maximum distance of 500 km to remove its dimensionality and ensure its value is between 0 and 1.

$$Nor_Distance(t) = \frac{Distance(t)}{500\ km},$$

To avoid division by zero when the distance between a cyclone and the sea ice grid point is zero, a small constant $\varepsilon = 10^{-4}$ is added to the denominator. This adjustment ensures the correctness of calculations without significantly affecting the results.

The SIC value of the sea ice at grid point (x, y) and time t is denoted as $SIC(x, y, t)$. Only the grid points with SIC $\geqslant$15% will be used to calculate exposure index. To calculate the exposure of the local sea ice grid point to passing cyclones within a specific time period, we sum the contributions of all n cyclones that pass through a 500 km radius of the grid point from 120 hours before to 120 hours after each timestep (per hour). This summation results in the index that quantifies the exposure of each sea ice grid point to passing cyclones at any moment. The exposure index is influenced by factors such as cyclone intensity ($Strength_{case(t)}$), distance from the cyclone to the sea ice grid point ($Distance(t)$), the number of cyclones within a 500 km radius ($\sum_{n=1}^{n=m}$) in a period ($\sum_{t-24}^{t+24}$), and the local SIC ($SIC(x, y, t)$). The interaction time between sea ice and cyclones is represented by the sum of times ($\sum_{t-24}^{t+24}\sum_{n=1}^{n=m}$) and the strength of cyclones over the sea ice is also computed in a 2-day period ($\sum_{t-24}^{t+24}\sum_{n=1}^{n=m} Strength_{case(t)}$).

In order to better compare the results between seasons, the exposure index at each time point is also normalized, with a min-max normalized to a range of 0~1.

$$Nor_Exposure(t) = \frac{Exposure(x,y,t) - Exposure_{min}}{Exposure_{max} - Exposure_{min}},$$

The maximum and minimum exposure values are derived from all grid points with SIC ≥15% over the entire 43-year period. The selected time window of ±1 day (48 hours) aims to capture as many passing cyclones as possible. This window is subjectively chosen and can be extended to ±3 or ±5 days, as shown in sensitivity tests (Figures S1 and S2). Cyclone speed indirectly affects the exposure index by influencing both the number of cyclones and their interaction time with sea ice. Thus, the exposure index serves as a valuable metric for quantifying cyclone influence on local sea ice and exploring regional differences in this relationship. Figure 1 illustrates $Nor_Exposure(t)$ at 15:00 on October 7, 2022, along with cyclone tracks over this 2-day period as an example.

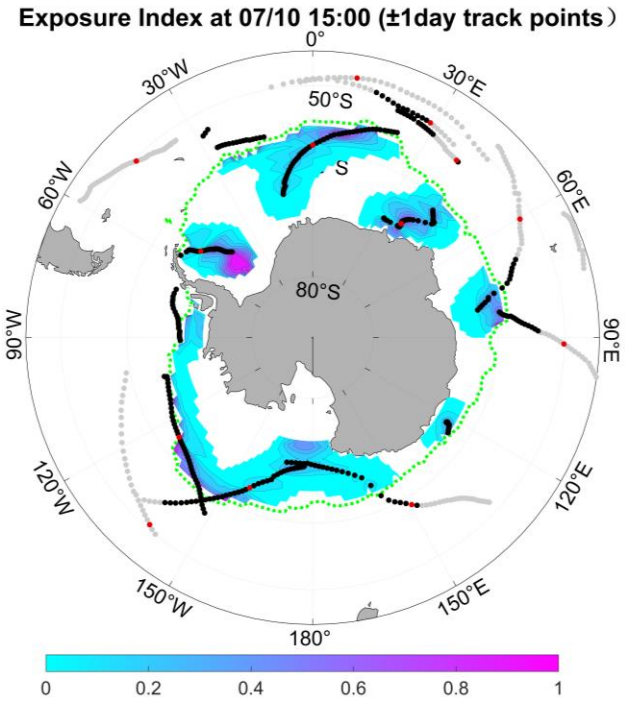

Figure 1. Normalized Exposure Index at 15:00 on October 7, 2022. Cyclone tracks are represented by dots. Gray dots represent cyclone track points far from the sea ice edge (green dashed line), while black dots indicate track points with sea ice within a 5° radius. Red dots mark the locations of cyclones at 15:00 on October 7, 2022.

2.4 Different sea ice response

The SIC anomaly field is re-gridded around the cyclone centers using B-spline interpolation to minimize the effects of meridional convergence in high latitudes. The SIC anomaly at each timestep is calculated as the difference between SIC values one day before and one day after. The mean SIC anomaly within 5° inward from the sea ice edge (indicated by the green dashed line) is calculated for a box region located to the west and east of the cyclone centers, as shown in Figure 2. This approach focuses on the main changes in the edge area and accommodates varying sea ice shapes. Based on the dominant anomalies observed on both sides of the cyclone, the cyclones are categorized into four groups: Both-I (SIC increase on both sides), Both-D (SIC decrease on both sides), WI-ED (SIC increase in the west and decrease in the east), and WD-EI (SIC decrease in the west and increase in the east). The SIC anomaly quantities for each cyclone are shown in Figure S3. The SIC changes on either side of the cyclone can reach up to 40%, with seasonal variations in the average SIC changes.

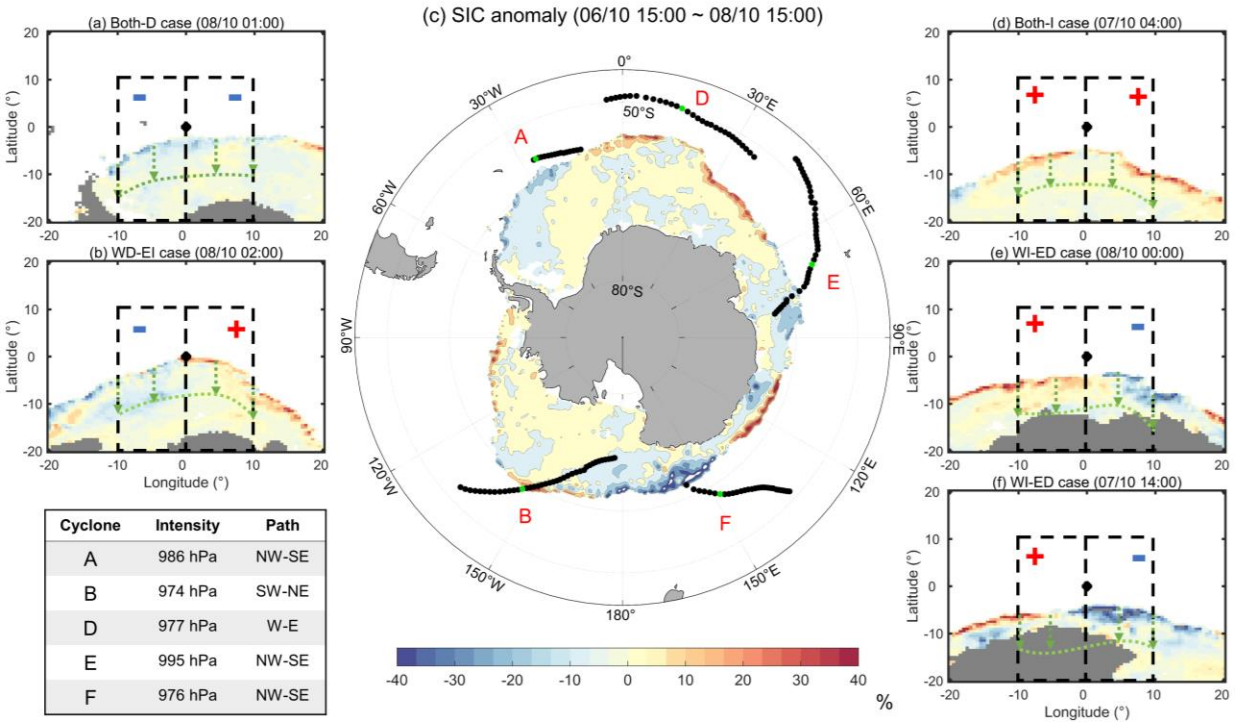

Cyclone	Intensity	Path
A	986 hPa	NW-SE
B	974 hPa	SW-NE
D	977 hPa	W-E
E	995 hPa	NW-SE
F	976 hPa	NW-SE

Figure 2. A schematic representation of four types of SIC responses to cyclones. (a) Both-D case (SIC decrease on both sides); (b) WD-EI case (SIC decrease in the west and increase in the east); (c) all cyclones with at least a 5% SIC anomaly from October 6 to October 8, 2022, with shaded areas indicating the SIC anomaly during the same period; (d) Both-I case (SIC increase on both sides); (e) and (f) WI-ED cases (SIC increase in the west and decrease in the east). The region between the sea ice edge and the green dashed line is used to calculate the mean SIC anomaly on the west or east flanks of cyclones. The intensity and path information for the five cyclone cases are summarized in the table.

3 Results

3.1 Variations in Antarctic sea ice and Southern Ocean cyclones

Antarctic sea ice undergoes a natural cycle characterized by gradual expansion and rapid retreat. The northward extension of the sea ice edge occurs from March to September, followed by a poleward retreat from October to February of the following year (Eayrs et al., 2019). This pattern results in a larger expanse of sea ice during winter (JJA) and spring (SON), and a smaller coverage during summer (DJF) and autumn (MAM), as shown in Figure 3a-d. Notably, regional differences exist in the seasonal shifts of sea ice extent. For example, the sea ice edge in the Weddell Sea (60°W-0°), Lazarev Sea (0-14°E), and Ross Sea (158°E-170°W) experiences more significant north-south seasonal variation compared to the IO and WPO sectors. These regions also exhibit larger standard deviations in the monthly positions of the sea ice edge (Figure 3g). The movement of sea ice in these areas is significantly influenced by katabatic winds and barrier

winds, which promote both sea ice production and export. However, their northward expansion is constrained by the oceanic frontal zone and storms (Nghiem et al., 2016).

The feature density of Southern Ocean cyclones exhibits a circular pattern (Figure 3a-d), gradually increasing from lower to higher latitudes. The highest cyclone frequency is observed around 60°S, gradually decreasing closer to the Antarctic continent. Peak storm activity occurs in the Indian Ocean and Western Pacific sectors year-round, consistent with the findings of Hoskins and Hodges (2005). Additionally, both the location and intensity of the storm track exhibit seasonal variation. During the retreat of sea ice (Figure 3c-d), the storm track shifts closer to the Antarctic continent, with heightened cyclone activity along the coast. As the sea ice advances (Figure 3a), the storm track shifts northward, particularly in the ABS and WS sectors, where it extends as far north as 60°S and 55°S, respectively. However, in the IO and WPO sectors, the location of the storm track remains relatively stable year-round, centered around 60°S.

Therefore, it is not surprising that the north-south movement of storm tracks over the Southern Ocean does not align with the expansion and retreat of the sea ice edge (Figure 3e). The storm track axis intersects the sea ice edge twice in the RS, ABS, and western WS in May and November, resulting in disparities in the number of cyclones (track points) located inside and outside the sea ice edge. The largest positive difference is observed in the 0-110°E region during MAM and remains positive year-round, while the central RS and ABS regions exhibit the largest negative difference in ASO, along with a significant inconsistent shift in the storm track and sea ice edge, with a relative distance ranging from -10° to 17° latitude. Note that this difference is heavily influenced by the position of the storm track, as the positions of the storm track in the WPO, ABS, and WS regions exhibit significant variability (Figure 3f), which is greater than that at the sea ice edge.

Given that cyclones with varying relative distances may have different impacts on sea ice, their relationship is also influenced by the differing proportions of cyclones inside and outside the sea ice edge. Therefore, it is valuable to categorize cyclone tracks located close to the sea ice edge, rather than considering cyclones spanning the entire Southern Ocean. The precise selection and classification of sea ice-linked cyclones based on their relative distance from the sea ice provide a new perspective on the trends and variations of cyclones associated with sea ice, in the context of global warming and the poleward movement of storm tracks.

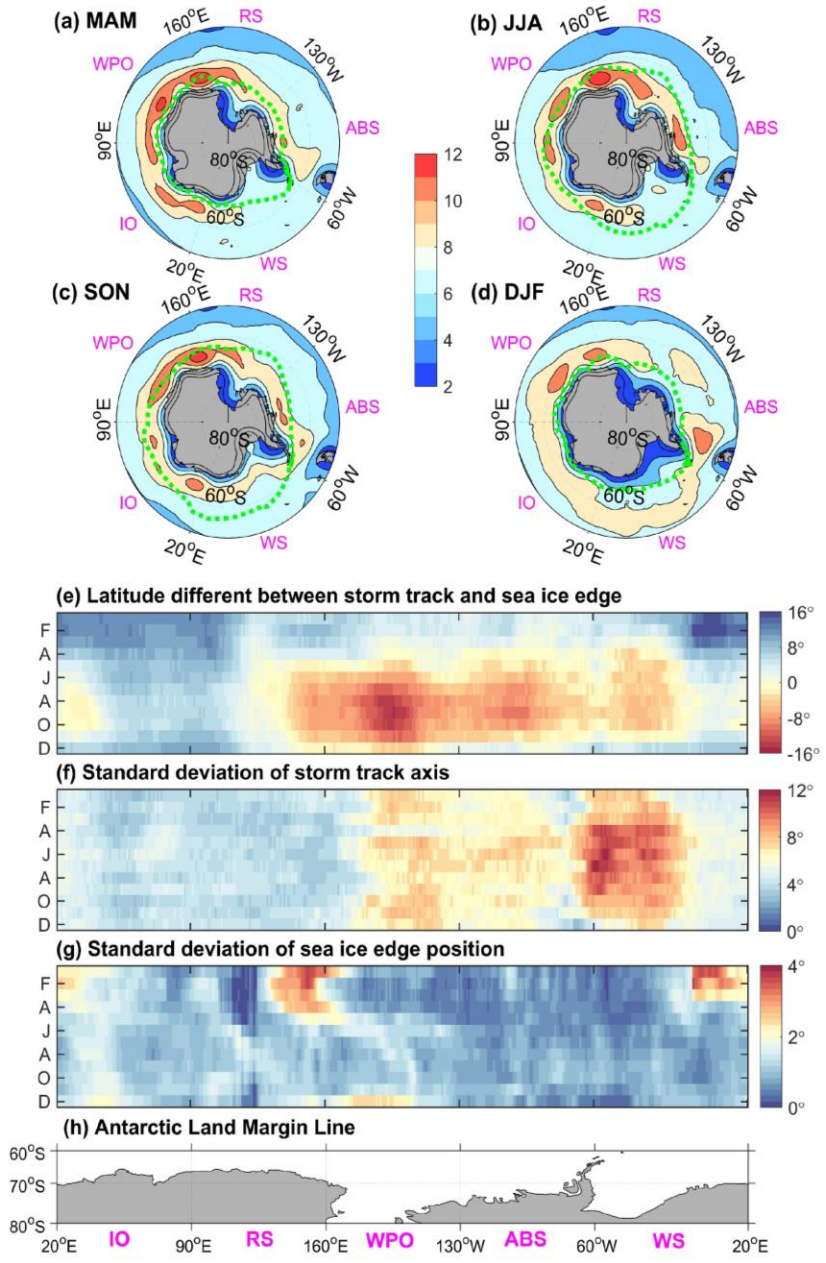

Figure 3. (a–d) Seasonal feature density of Southern Ocean cyclones (shaded) and the mean sea ice edge (SIC ≥ 0.15, green contour). Unit: per season. (e) (e) Monthly variation in the latitudinal difference between the storm track axis (latitude of maximum density in each meridian) and the sea ice edge at the same longitude, calculated as the former minus the latter. (f) Monthly variation in the standard deviation of the storm track axis. (g) Monthly variation in the standard deviation of the sea ice edge position. (h) The edge of the Anarctic continent.

3.2 Trends of sea ice and ice-linked cyclones

The expansion of Antarctic sea ice might increases its interaction with mid-latitude cyclones. Our analysis reveals that the average latitude of the full tracks of ice-linked cyclones, as well as their tracks over ice, follows the trends of sea ice edge movement—showing a northward shift before 2014 and a southward shift afterward. However, the trends in the average latitude of cyclone genesis and lysis differ from those of sea ice (not shown).

Further examining the latitude of the sea ice edge (IEL) within each sub-region, we find more pronounced trends before 2015 than over the entire period from 1980 to 2022 (Figure 4a). Some significant trends from 1980 to 2015, such as the northward shift of IEL in the RS region, lose their statistical significance when data is extended to 2022. However, the southward IEL trend in ABS during DJF and MAM, as well as the northward trend in WPO (RS) during MAM (JJA), remain significant after 2015, consistent with previous studies (Maksym 2018). Notably, the largest northward trends in RS have weakened, while those in WS have reversed southward. IEL trends in IO and WPS are relatively small, indicating that inter-decadal variations in Antarctic sea ice extent are primarily driven by the southward trend in ABS and the northward trend in RS.

Regional sea ice trends are driven by atmospheric and oceanic processes. The summer Ross Sea decline is linked to an enhanced anticyclonic SAM pattern, while strengthened SAM asymmetry in winter and spring influences SIC changes across Antarctica (Schroeter et al., 2023). The extreme El Niño (Dec 2015–Feb 2016) triggered persistent ocean warming in the Bellingshausen, Amundsen, and eastern Ross Seas (Stuecker et al., 2017; Parkinson, 2019). Sea surface temperature (SST) trends are also consistent with the reversal of sea ice trends in these regions. However, in Weddell Sea and some areas of the East Antarctica, sea ice changes are mainly driven by weather-scale and teleconnection processes, with limited influence from large-scale SAM variations (Schroeter et al., 2023).

Therefore, investigating the trend of ice-linked cyclones around Antarctica is crucial. In Figure 4c, about 40% of the tracks of Southern Ocean cyclones will affect the sea ice and half of them will enter the sea ice edge. The percentage is different across subregions but positive trends are observed in the number of ice-linked cyclones in most regions (Figure 4b), particularly during the MAM and DJF when the sea ice extent is relatively small (Figure 3a and 3d). The WS sector exhibits the largest increase in cyclone numbers, while the RS has the smallest and non-significant trend for all four seasons. Notably, the outside cyclones in the ABS region also have a significant increasing trend in JJA and SON, which is not seen anywhere else in these seasons. Only the ABS region exhibits a significant decreasing trend in the number of inside cyclones in MAM, which might be associated with the southward trend of IEL in ABS. Predictably, the retreat of the sea ice edge leads to a reduction in the number of cyclones within ice-covered areas. However, this common assumption may not be true for the RS and WS regions. For example, the IEL in the WS region shows a weak southward trend, yet there is still a positive trend in the number of inside cyclones in this region, indicating cyclones may be moving southward in concert with the southward-moving ice edge.

On a decadal timescale, increasing trends are observed in both the number of outside and inside cyclones, while sea ice extent shows an increasing trend in the IO, WPO, and RS regions, but a decreasing trend in the ABS and WS regions. Significant correlations are found

only between the IEL and the number of inside cyclones (not shown), rather than with outside cyclones. This suggests that no meaningful statistical relationship exists on a decadal timescale, even though the cyclones were well-tracked and selected. Instead, the relationship between cyclones and sea ice may be significant only on shorter timescales in specific regions. The regional and seasonal variations in ice-linked cyclone characteristics and sea ice conditions further complicate their relationship. Understanding both cyclone characteristics and regional sea ice variability is essential for addressing this issue.

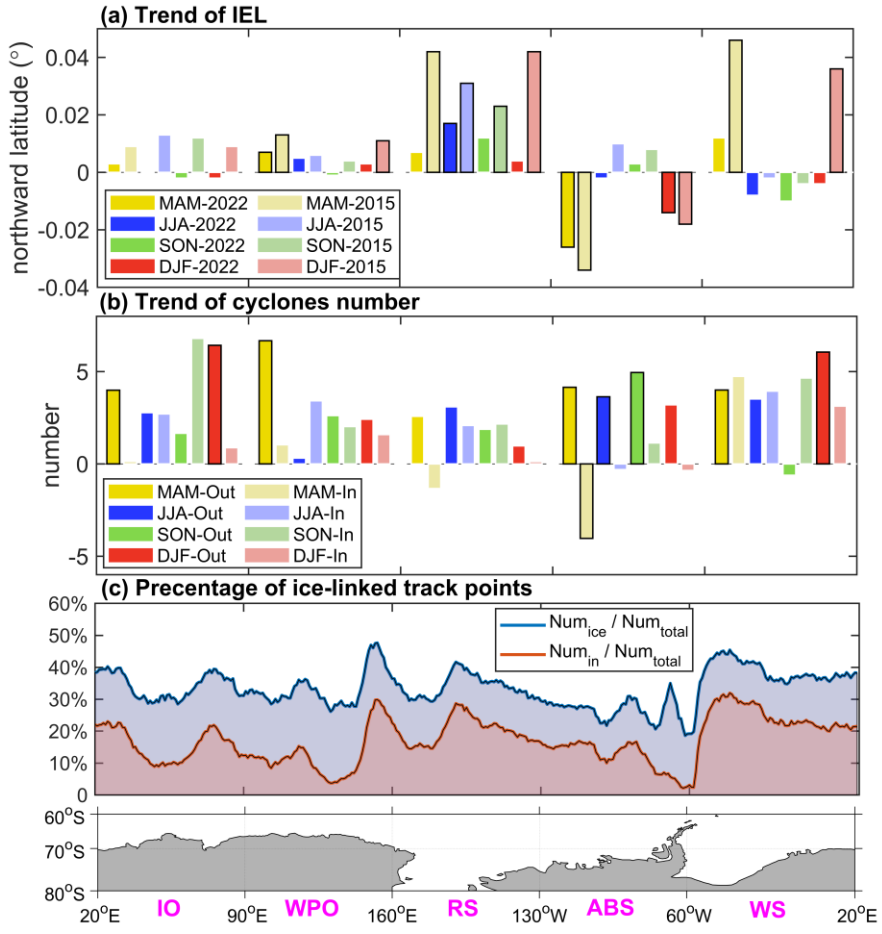

Figure 4. (a) Trends in the latitude of the sea ice edge in each subregion from 1980 to 2015 (light-colored bars) and 2022 (dark-colored bars). Positive (negative) values indicate a northward (southward) shift trend. (b) (b) Trends in cyclone frequency inside and outside the sea ice edge in each subregion from 1980 to 2022. Bars indicating significant trends are outlined in black (t-test: 95% confidence level). (c) The blue line represents the percentage of ice-linked track points at each meridian relative to all track points. The red line represents the percentage of track points inside the sea ice edge.

3.3 Features of ice-linked cyclones

According to the methods described in methods section, we investigate the characteristics of cyclones by dividing them into inside and outside groups to compare the differences between cyclones inside and outside the sea ice edge. Surprisingly, the number of outside cyclones remains fairly consistent across various seasons in most regions, except for a 10% larger number in the WPO sector in MAM and the ABS sector in SON (Figure 5a). The seasonal latitudinal shift of the sea ice edge appears to primarily impact the number of inside cyclones (Figure 5e). Larger seasonal differences in the number of inside cyclones are observed not only in regions with extensive sea ice (RS and WS) but also in areas with narrower sea ice extent (IO and WPO).

Seasonal and regional differences also exist in the strength (MSLP minima) of cyclones (Figure 5b). A similar double peak can be seen in the WPO and ABS sectors in JJA and SON. Conversely, cyclones exhibit stronger intensity in JJA than in SON in the WS-IO sector. Summer (DJF) cyclones are notably less intense than their winter (JJA) counterparts in general. Notably, a single peak in cyclone intensity is observed in the ABS region for outside cyclones in summer, indicating that the cyclones here maintain stronger strength throughout the year. Furthermore, the significant positive trend in the number and strength of cyclones in the ABS region, along with their increased southward movement speed, may contribute to the notable decline in sea ice in this region compared to others (Figure 4a).

In addition to the sea ice response to the number and strength of cyclones, sea ice may also respond to varying cyclone translational speeds and trajectories. Slow-moving cyclones tend to engage with sea ice over extended durations, resulting in more pronounced dynamic and thermal effects on the ice. Outside cyclones generally move at speeds within a range of 7-18 m/s (Figure 5c). The mean speed, partially dependent on the number of cyclones, also shows regional and seasonal differences. The highest mean speeds manifest at 160°E during winter. The peaks of the mean speed align with regions where sea ice extends northward, such as the Drake Passage and Prydz Bay. Cyclones west of the Antarctic Peninsula typically have low speed and a larger northward component in their motion. Most of them accelerate when they pass through the Drake Passage and then turn southward (Figure 5d). The largest southward component appears at 110°E, coinciding with peaks in number and strength. This implies that cyclones in this region are more likely to intrude extensively into the sea ice, thereby imposing a more severe impact on the ice. Another area that may have a severe impact is located in the ABS area, where cyclones have large strength, slow speed, and large southward moving direction.

The seasonal variation of the sea ice edge has a great impact on the average feature of inside cyclones, especially in the regions that have wide sea ice areas such as the RS, WS regions, and Prydz Bay (Figure 5e). The large number of inside cyclones in these regions may weaken the peak value of cyclone features, especially for the mean speed and southward component of moving direction. Generally, their speed is also slower entering the sea ice edge due to the influence of the continent and the circumpolar easterly winds (Figure 5g). Similar to outside cyclones, there is an acceleration in the speed of inside cyclones west of the Antarctic Peninsula accompanied by a pronounced northward motion component. Another northward passage occurs around the primary meridian, beyond which most cyclones move south (Figure 5h). The

three peaks of the number of inside cyclones around 160°E, 170°W, and 45°W correspond to the three main cyclogenesis regions along the coast (Figure 5e), accompanied by frequent cold air outbreak events and strong katabatic winds (Parish & Cassano, 2003; Bromwich et al., 2011; Papritz et al., 2015). In other regions, the difference in numbers between JJA and DJF is mostly attributed to the expansion of the sea ice extent. Except for the larger numbers than outside cyclones, the intensity of inside cyclones also has two peaks around 90°E and 130°W and they last for two and three seasons respectively (Figure 5f). Cyclones within the narrow sea ice band in the IO-WPO sector do not have enough time and space to reach higher intensities in MAM.

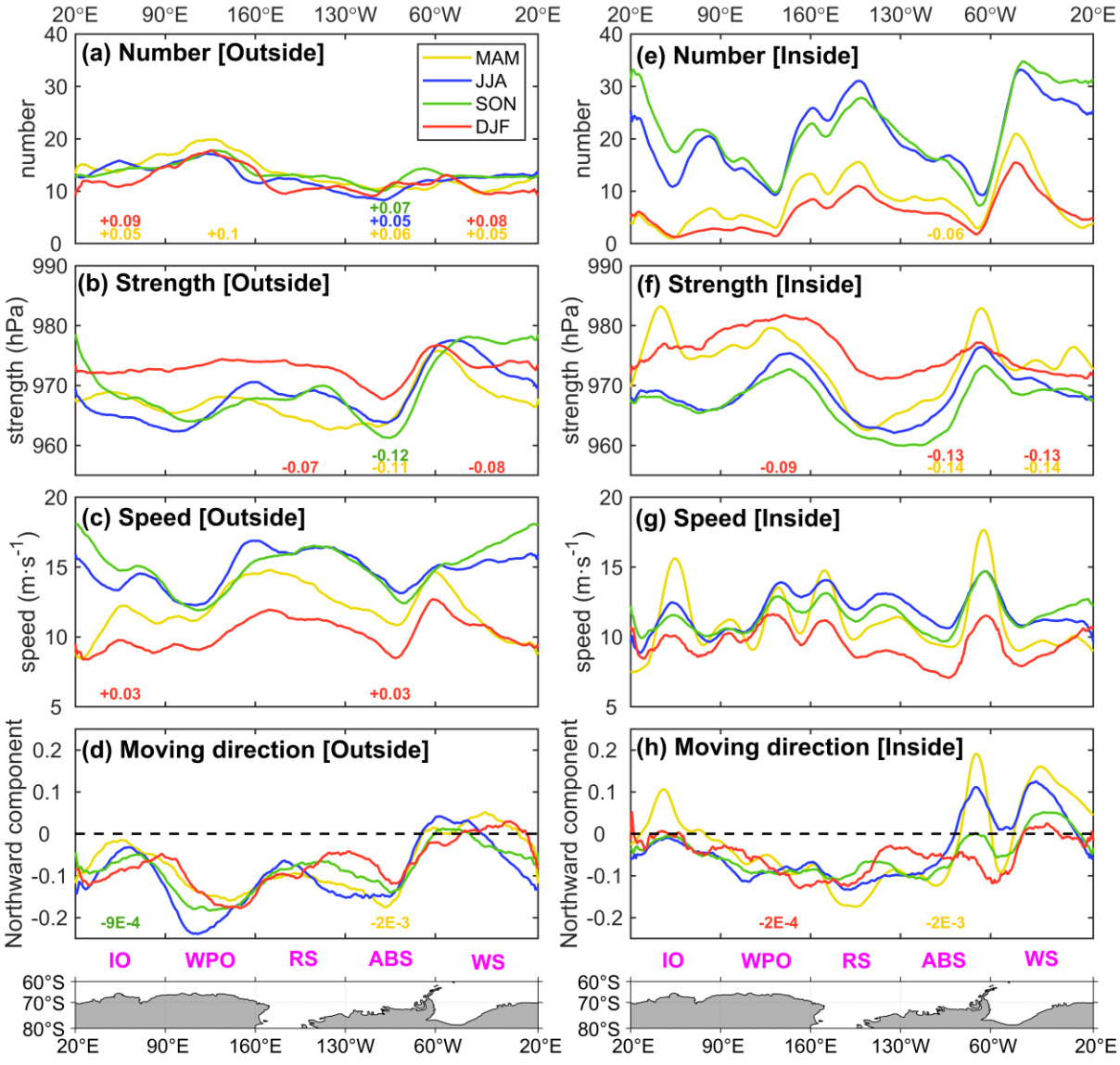

Figure 5. Meridional-mean values of (a & e) cyclone count, (b & f) strength, (c & g) speed, and (d & h) moving direction (northward component) for ice-linked cyclones outside the sea ice edge (a-d) and inside the sea ice edge (e-h) during MAM (yellow line), JJA (blue line), SON (green line), and DJF (red line). Only smoothed results using a 30-point moving average are shown. Significant

trends (passing the 95% t-test level) are shown below the lines, with colors corresponding to the respective seasons. Unit: per year.

3.4 Index of sea ice exposure to cyclones

To comprehensively analyze the seasonal and regional relationship between cyclones and sea ice, an exposure index has been developed to assess the impact of cyclones on sea ice (Data and Method 2.3). The index accounts for the number and strength of passing cyclones, the interaction time between sea ice and cyclones, and the local SIC. Typically, sea ice in areas with low SIC and frequent cyclone activity, such as the marginal ice zone (MIZ: $0.15 < SIC < 0.75$), is more susceptible to severe impact by cyclones. Therefore, a high-exposure belt is expected along the sea ice edge in all four seasons, although seasonal and regional differences exist.

The highest exposure value is observed in the WPO sector, driven by the local feature of a larger number of slow-moving cyclones and the largest southward component in their movement direction (Figure 5a-d). The interaction time increases when there are a large number of slow-moving cyclones (Figure 6e-h). Cyclones with greater strength are likely to be more destructive to sea ice, particularly in the MIZ. When cyclones move across the sea ice edge and enter the interior of the sea ice cover where $SIC > 0.9$, the exposure index decreases despite longer interaction times and higher mean cyclone strength. This can be seen in the RS and WS basins typically (Figure 6j-k). Slow-moving cyclones near the coast also increase the interaction time. The exposure index in the RS and WS regions shows similar seasonal variations. Due to the rapid retreat of sea ice in these two regions during DJF, more low-density ice areas emerge, leading to a wider high-exposure area instead of a narrow belt seen in other seasons (Figure 6d).

The condition of the sea ice strongly influences the index. The Antarctic sea ice has a rapid growth in MAM and a decline in DJF. In these two seasons, the exposure value is higher than that in JJASON because more grid points with low SIC in MAM may be easily affected by the cyclones. In general, SIC dominates the seasonal variation of the exposure index, while cyclones dominate the regional differences in the exposure index. However, this is not an absolute conclusion. For example, the small number of summer cyclones results in a lower exposure index in the MIZ during DJF compared to other seasons, while the thick, old ice in the frontal ice zone of the RS protects the sea ice from further cyclone impacts during JJA. Although cyclones with different characteristics in different seasons cause significant differences in mean strength over sea ice and interaction time, the response in the range and depth of high exposure in the MIZ is limited after considering sea ice concentration. This variation in the exposure index may help explain why the relationship is regional and seasonal, as well as identify the most noteworthy season for each subregion.

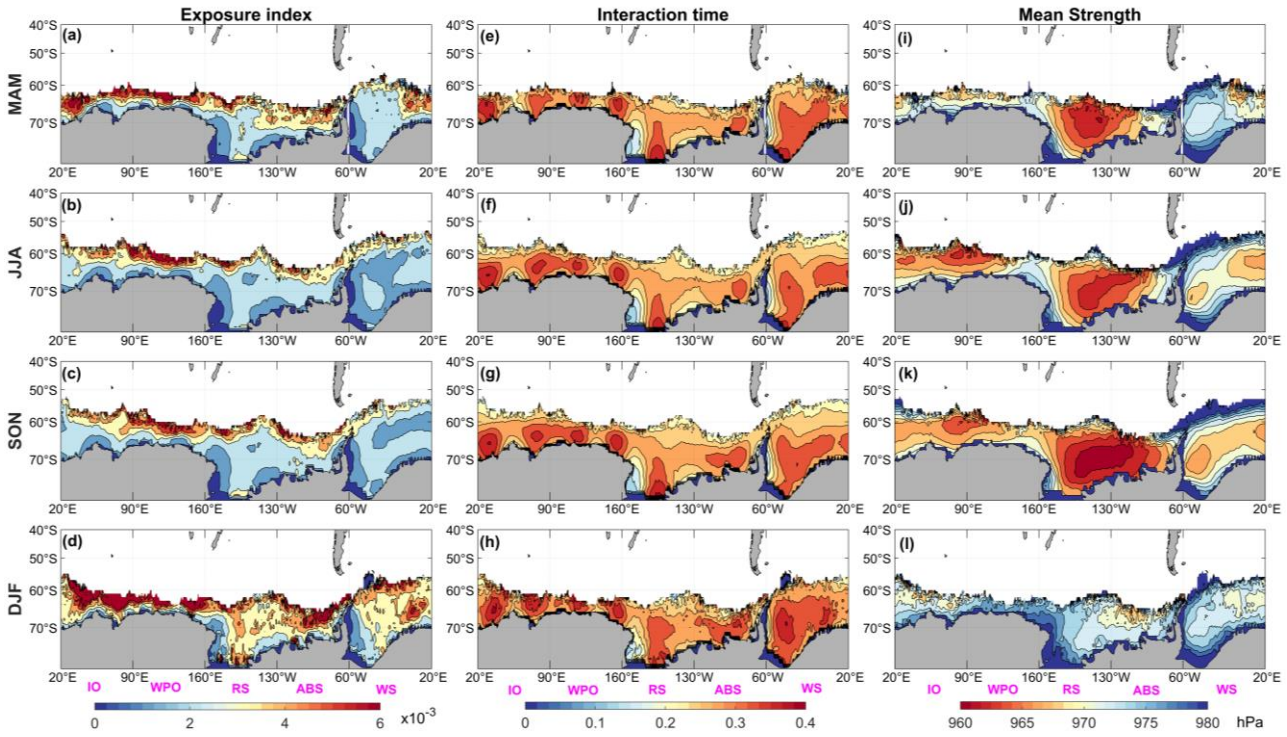

Figure 6. Panels (a–d) show the seasonal distributions of the normalized exposure index. Panels (e–h) present the mean normalized interaction time, calculated by dividing by 48 hours for ±1-day periods. Panels (i–l) display the mean strength of these cyclones. Each row corresponds to a different season, with season markers indicated on the far left.

3.5 SIC responses to cyclones

Following the analysis of cyclone characteristics and sea ice exposure above, regional and seasonal differences in the exposure of sea ice to cyclones have been identified. However, it remains uncertain whether the passage of a cyclone will lead to an increase or decrease in local SIC. To address this, it is necessary to examine the cumulative impact of each cyclone on the local sea ice using a SIC anomaly field around the cyclone center over a ±1 day period. Given the limited movement of the cyclone, sea ice anomalies within ±1 day can mainly be attributed to the cyclone itself. September ice-linked cyclones are selected for this composite analysis to mitigate the influence of seasonal sea ice growth/retreat and missing values over land on the results. These cyclones are categorized based on positive and negative sea ice anomalies on their eastern and western sides (Data and Method 2.4).

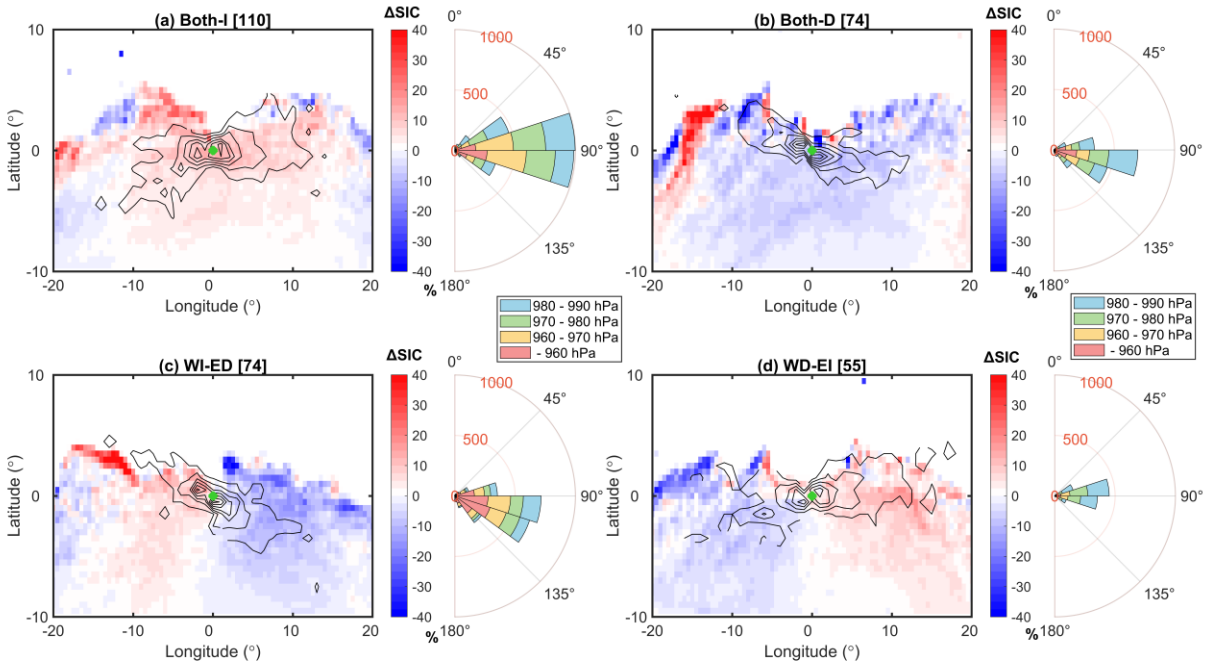

Figure 7. Composite results (shaded) of isolated cyclones in September, categorized as (a) Both-I, (b) Both-D, (c) WI-ED, and (d) WD-EI sea ice anomalies within ±1 day. Track density is outlined in black contours, and cyclone centers are marked with green dots. The adjacent wind rose chart illustrates cyclone intensity (MSLP) and movement direction. The number of cyclones included in the composite analysis is indicated in square brackets in the title.

The composite focuses on isolated cyclones to avoid the influence of additional cyclones upstream or downstream on the composite results. Figure 7 shows the SIC composite results for four types of cyclones and their track features. On average, an isolated cyclone causes an anomaly of up to ±40% in SIC within two days, with significantly large anomalous values at the sea ice edge. In general, cyclones have a greater impact on the sea ice edge than on the interior, manifested by southward movement and extrusion of sea ice on the east side and northward movement with internal ice growth on the west side of the cyclone center. This results in a positive SIC anomaly on the west side and a negative SIC anomaly on the east side (WI-ED), with thermodynamic effects from the cyclonic circulation further reinforcing this pattern. The cyclone path influences the shape of the sea ice edge and anomaly distribution, with different paths observed in various cases (e.g., NW-SE path for Both-D and WI-ED cases, W-E path for Both-I and WD-EI cases).

The wind rose chart indicates that WI-ED cyclones are significantly stronger than Both-D cyclones during their interaction with sea ice, with nearly half of the time steps showing intensities below 970 hPa and one-third below 960 hPa. This strength difference explains the positive anomaly on the west side of WI-ED cyclones but not Both-D cyclones, even though both have similar NW-SE paths moving towards the interior of the sea ice (Figure 7b and 7c). A stronger WI-ED cyclone can drive more intense cold advection towards the equator on the west side

(Figure 8c), leading to rapid sea ice growth. In contrast, the weaker Both-D cyclone lacks favorable conditions for sea ice growth on its western side. There is either no or weak cold advection and less surface sensible heat flux (SSHF) on the western side of the Both-D cyclone (Figure 8b and 8f). In terms of maximum wind speed and significant wave height, the distribution pattern is similar for both cyclones, differing primarily in intensity (Figure 8i-j and 8n-o). Thus, it is reasonable to infer that along an NW-SE path, a strong cyclone most likely induces a WI-ED sea ice response, while a weak cyclone typically results in a Both-D response. The key factor distinguishing them is the strength of cold advection and negative SSHF on the western side. Both have large warm advection and positive SSHF on the eastern side, which distinguishes them from the other two types of cyclones.

Comparing the Both-I and WD-EI cases, Both-I generally follows a W-E path (Figure 7a). Along this path, the negative anomaly on the eastern side is partially offset by the positive anomaly from offshore winds on the western side as the cyclone moves eastward, resulting in an east-west increasing anomaly pattern over two days. As the cyclone moves eastward, the original negative anomaly on the eastern side is offset. In terms of sensible heat flux, only the western side exhibits a larger negative sensible heat flux, while the eastern side is close to 0 (Figure 8e). These results are opposite to those observed in Both-D cyclones (Figure 8f). The WD-EI cases also follow a W-E path but have more northward components (Figure 7d). Most WD-EI cases have their genesis at the sea ice edge and move eastward afterward, resulting in significantly more trajectory points on the eastern side than on the western side. Hence, the negative anomaly on the western side may not be attributed solely to the cyclone itself. In Figure 8d, the range of cold and warm advection for this cyclone type is much smaller than that for the other three types. These cyclones, which develop by baroclinicity from air-ocean temperature differences at the ice edge, are typically small- to mesoscale, with weaker intensity (Figure 7d) and cause the smallest wind speeds and lowest wave heights among the three types (Figure 8l and 8p). This also raises the question of whether such an abnormal WD-EI response is caused by the cyclone itself or the background circulation, as evidenced by the stronger warm advection on the left and cold advection on the right outside the cyclone's circulation, compared to the cyclone itself (Figure 8d).

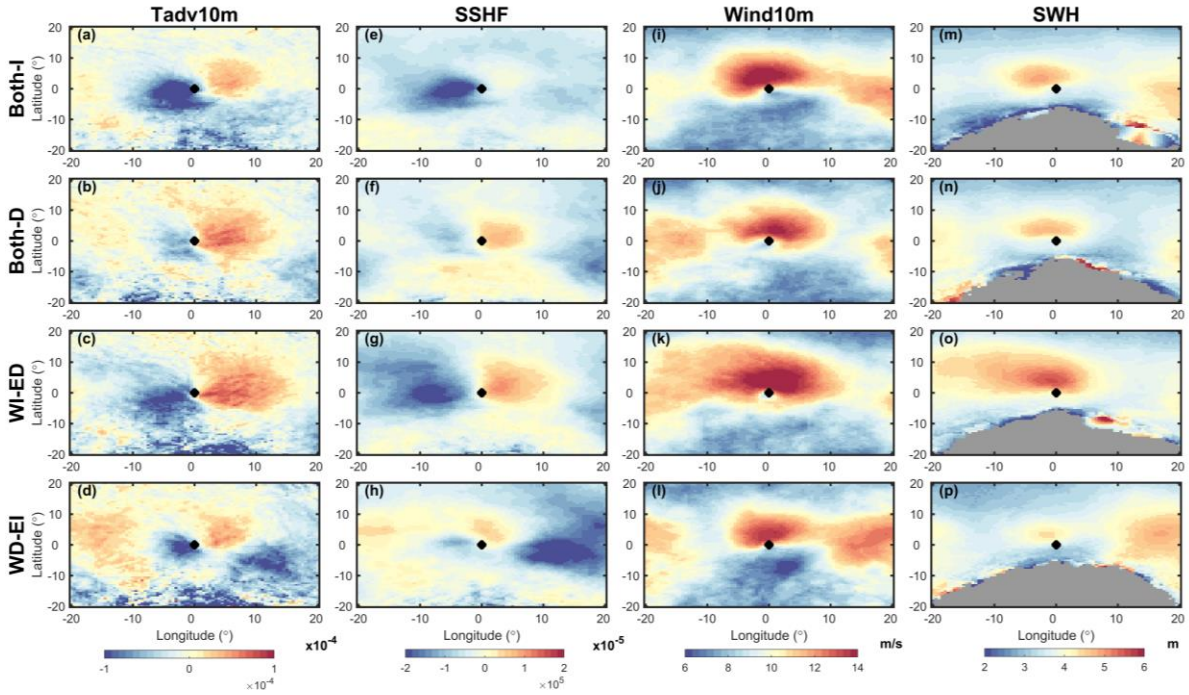

Figure 8. Composite results (shaded) of environmental factors for different types of isolated cyclones in September. Panels (a–d) depict temperature advection at 10m, while panels (e–h) illustrate surface sensible heat flux. Panels (i–l) present wind speed at 10m, and panels (m–p) display significant wave height. Cyclone centers are marked with black dots.

4 Discussion

By categorizing cyclones based on SIC anomalies in this study, we provide a reasonable explanation for the weak correlation between Antarctic sea ice and cyclones on interannual and decadal scales. The relationship between cyclones and sea ice varies annually due to the differing proportions of the four types of SIC anomalies among cyclones. It is not straightforward to predict whether sea ice will increase or decrease abnormally in years with unusually high or low cyclone activity. The annual cycle of cyclone impacts on SIC is influenced by variations in cyclone intensity and the sea ice conditions they traverse (Aue et al., 2023a). A high number of cyclones does not necessarily indicate extreme sea ice extent. However, case studies on the relationship between cyclones and extreme sea ice reduction events (e.g., Turner et al., 2017; 2022 in Antarctica; Simmonds and Rudeva, 2012; Zhang et al., 2013 in the Arctic) provide confidence in continuing to explore this relationship. At the very least, they allow us to summarize differences in cyclone characteristics and transport factor fields during the early stages of extreme sea ice years. This is particularly important in the context of global warming and the recurring record lows in Antarctic sea ice. Future research can begin by examining seasonal changes in sea ice. Based on previous findings, the circumpolar trough can influence sea ice growth (Eayrs et al., 2019), while cyclone location and local wind fields can drive extreme changes in local sea ice (Wang et al., 2014). In our other studies, we have found a relationship between the monthly advance speed of the sea ice edge and the number of the four types of cyclones. However, it remains necessary to quantify

622 the net contribution of cyclones to sea ice growth and melting, beyond their role in the spatial
623 redistribution of sea ice.

624 Further investigation of the relationship between cyclones and extreme sea ice requires
625 careful screening of cyclones based on their characteristics, including their paths and intensities
626 as well their wind speed and direction. The current research still has some limitations, such as
627 the potential impact of ERA5 data bias, which can benefit from the comparative validation with
628 multiple data sets; The T42 spatial filtering used in cyclone tracking retains only synoptic scale
629 signals, resulting in the lack of small- and mesoscale cyclones in the dataset. These small-size
630 cyclones are mostly linked to cold air outbreaks and are also closely related to sea ice (Irving et
631 al., 2010); Only eastward-moving cyclones were selected in our study because they accounted
632 for 75% of all track points and had a significant increasing trend. In fact, the influence of different
633 directions of the cyclone on the anomalous sea ice concentration is significant, because its
634 asymmetrical wind field structure is accompanied by asymmetrical swells. In addition, the speed
635 of the cyclone may cause different sea ice anomalies. The fast eastward moving cyclone may have
636 little effect on sea ice, the positive sea ice anomaly caused by the offshore wind to the west will
637 offset the negative sea ice anomaly caused by the onshore wind to the east at the previous
638 moment, and the final accumulation will be a small impact. Local sea ice changes can also result
639 from the cumulative effects of multiple cyclones, particularly during winter when cyclone activity
640 intensifies. Dynamic mechanisms dominate the SIC response during rapid succession of cyclones,
641 while longer gaps between cyclones before and after allow thermodynamic effects to lead in
642 refreezing (Aue et al., 2023b). The multiple impact of cyclone clusters are also need to further
643 investigate. Therefore, we are interested in whether slow and strong cyclones and cyclone
644 clusters cause long-term changes in sea ice, since the number of such cyclones may have a
645 stronger relationship with the extreme sea ice extent events. It is quite challenging to identify
646 which features of cyclones lead to long-term changes in sea ice, resulting in extreme SIE events
647 in the following month or season, and finding reasonable physical mechanisms for this
648 correlation should be a focus of future work.

649

650 **5 Conclusions**

651 The sea ice around Antarctica undergoes a natural cycle of expansion and retreat, with
652 larger areas covered by sea ice during winter (JJA) and spring (SON), and smaller areas during
653 summer (DJF) and autumn (MAM). Regional variations exist in the positioning of the sea ice edge,
654 particularly in the Lazarev Sea and the Ross Sea, where significant north-south variations are
655 observed. Meanwhile, the tracks of Southern Ocean cyclones follow a circular pattern, with the
656 highest frequency observed around 60°S. The storm track shifts closer to the Antarctic continent
657 during the sea ice retreat period (ONDJF) and extends northward during the sea ice advance
658 period (MAMJJAS). However, the south-north shift of the storm track does not coincide with the
659 expansion and retreat of the sea ice edge, resulting in disparities in the number of track points
660 inside and outside the sea ice edge. Here, we show that both inside and outside cyclone track
661 points exhibit an increasing trend on a decadal timescale, although the increasing trend of sea
662 ice extent reverses after 2015. The correlation coefficient analysis further reveals no significant

663 relationship between the number of outside cyclones and the latitude of sea ice edge on a long-
664 term timescale. The shifting sea ice edge mainly affects the number of track points within the ice
665 edge, while the number of track points outside remains similar across most seasons. The strength
666 of cyclones also varies between regions and seasons, with wider sea ice areas allowing for further
667 development and longer lifetimes of cyclones inside the ice edge. The speed and direction of
668 cyclone movement should also be considered in the study of the relationship between cyclones
669 and sea ice.

670 Therefore, an exposure index was designed based on the features of cyclones, local sea
671 ice conditions, and the interaction time between them. A high-exposure belt exists along the sea
672 ice edge throughout the year. Regions with low SIC and frequent cyclones are more susceptible
673 to cyclone impacts. Regional and seasonal variations in the exposure index can be explained by
674 the features of cyclones. For example, the highest exposure occurs in the WPO sector due to local
675 cyclones with larger numbers, slower speeds, and southward movement. Generally, cyclones
676 with slower speeds have a greater impact on sea ice due to longer interaction times. The
677 exposure index map helps explain the regional and seasonal relationship between cyclones and
678 sea ice, highlighting noteworthy seasons for each subregion.

679 On this basis, we further focus on the response of SIC to cyclones at the sea ice edge. On
680 average, isolated cyclones can induce ±40% SIC anomalies within two days, particularly at the sea
681 ice edge. Along the same NW-SE path, stronger cyclones drive intense cold advection, causing a
682 WI-ED response, while weaker cyclones result in a Both-D response due to favorable conditions
683 for west-side sea ice growth. The W-E path of cyclones produces a Both-I response, with the
684 negative anomaly on the eastern side of the cyclone offset by the positive anomaly after the
685 cyclone passes through. In general, SIC anomaly distribution depends on the cyclone path,
686 intensity, and environmental factors such as temperature advection and surface sensible heat
687 flux. This provides a new perspective on short-term changes in sea ice driven by cyclones.

688 Overall, the variations in Antarctic sea ice and Southern Ocean cyclones are complex and
689 interconnected. The impact of cyclones on sea ice throughout their entire life cycle is dynamic,
690 depending on the characteristics and conditions of the sea ice below. Understanding the
691 dynamics and interactions between sea ice and cyclones, including the impact of cyclones on
692 ocean and sea ice properties, is crucial for accurately assessing their effects on sea ice extent and
693 variability. The trends in the number of cyclones and the latitude of the sea ice edge show
694 significant seasonal and regional variation, as does the proportion of cyclones outside and inside
695 the sea ice edge. The findings presented here provide valuable insights into these relationships,
696 which can contribute to understanding recent trends and variability in Antarctic sea ice, its
697 seasonal and regional characteristics, and the future effects of global warming and the poleward
698 shift of storm tracks on Antarctic sea ice.

699

700 **Acknowledgments**

This study was supported by the National Natural Science Foundation of China (No. 41941009) and the Southern Marine Science and Engineering Guangdong Laboratory (Zhuhai) (Nos. SML2023SP217, SML2023SP219, SML2022SP401). We thank Kyle Clem at Victoria University of Wellington for useful comments on the paper.

Open Research

Hourly ERA5 data are available at Hersbach et al. (2023a, 2023b) and they can be downloaded from Climate Data Store of Copernicus Center (Two datasets: ERA5 hourly data on single levels from 1940 to present and ERA5 hourly data on pressure levels from 1940 to present). Southern Ocean cyclone dataset is available at Zhong et al. (2022). The code for the cyclone detection and tracking algorithm can be found at https://gitlab.act.reading.ac.uk/track/track.

References

Aue, L., Vihma, T., Uotila, P., & Rinke, A. (2022). New insights into cyclone impacts on sea ice in the Atlantic sector of the Arctic Ocean in winter. *Geophys. Res. Lett.*, *49*, e2022GL100051. https://doi.org/10.1029/2022GL100051

Aue, L., & Rinke, A. (2023a). Cyclone impacts on sea ice concentration in the Atlantic Arctic Ocean: Annual cycle and recent changes. *Geophys. Res. Lett.*, *50*, e2023GL104657. https://doi.org/10.1029/2023GL104657

Aue, L., Röntgen, L., Dorn, W., Uotila, P., Vihma, T., Spreen, G., & Rinke, A. (2023b). Impact of three intense winter cyclones on the sea ice cover in the Barents Sea: A case study with a coupled regional climate model. *Front. Earth Sci.*, *11*, 1112467. https://doi.org/10.3389/feart.2023.1112467

Bromwich, D., Steinhoff, D., Simmonds, I., Keay, K., & Fogt, R. (2011). Climatological aspects of cyclogenesis near Adélie Land, Antarctica. *Tellus*, *63A*, 921–938. https://doi.org/10.1111/j.1600-0870.2011.00537.x

Carleton, A. (1983). Variations in Antarctic sea ice conditions and relationships with Southern Hemisphere cyclonic activity, winters 1973-77. *Arch. Meteorol. Geophys. Bioclimatol. Ser. B Theor. Appl. Climatol.*, *32*, 1–22. https://doi.org/10.1007/BF02269387

Carleton, A., & Carpenter, D. (1989). Intermediate-scale sea ice—atmosphere interactions over high southern latitudes in winter. *GeoJournal*, *18*, 87–101. https://doi.org/10.1007/BF00722392

Clancy, R., Bitz, C. M., Blanchard-Wrigglesworth, E., McGraw, M. C. & Cavallo, S. M. (2022). A cyclone-centered perspective on the drivers of asymmetric patterns in the atmosphere and sea ice during Arctic cyclones. *J. Climate, 35,* 73–89. https://doi.org/10.1175/JCLI-D-21-0093.1

Clem, K., Massom, R., Stammerjohn, S., & Reid, P. (2022). Antarctic sea ice #2: Biological importance. *Antarctic Environments Portal*. https://doi.org/10.48361/8TKY-2793

Dare, R., & Atkinson, B. (1999). Numerical modeling of atmospheric response to polynyas in the Southern Ocean sea ice zone. *J. Geophys. Res.*, *104*, 16691–16708. https://doi.org/10.1029/1999JD900137

Eastwood, S., Lavergne, T., & Tonboe, R. (2014). Algorithm theoretical basis document for the OSI SAF global reprocessed sea ice concentration product, version 1.1. EUMETSAT Satellite Application Facilities, Darmstadt, Germany.

Eayrs, C., Holland, D., Francis, D., Wagner, T., Kumar, R., & Li, X. (2019). Understanding the seasonal cycle of Antarctic sea ice extent in the context of longer-term variability. *Reviews of Geophysics*, *57*, 1037–1064. https://doi.org/10.1029/2018RG000631

Eayrs, C., Li, X., Raphael, M., & Holland, D. (2021). Rapid decline in Antarctic sea ice in recent years hints at future change. *Nat. Geosci.*, *14*, 460–464. https://doi.org/10.1038/s41561-021-00768-3

Finocchio, P., Doyle, J., Stern, D., & Fearon, M. (2020). Short-term impacts of Arctic summer cyclones on sea ice extent in the marginal ice zone. *Geophys. Res. Lett.*, *47*, e2020GL088338. https://doi.org/10.1029/2020GL088338

Finocchio, P., Doyle, J., & Stern, D. (2022). Accelerated sea ice loss from late summer cyclones in the new Arctic. *J. Climate*, *35*, 7751–7769. https://doi.org/10.1175/JCLI-D-22-0315.1

Francis, D., Eayrs, C., Cuesta, J., & Holland, D. (2019). Polar cyclones at the origin of the reoccurrence of the Maud Rise Polynya in austral winter 2017. *J. Geophys. Res.: Atmospheres*, *124*, 5251–5267. https://doi.org/10.1029/2019JD030618

Godfred-Spenning, C., & Simmonds, I. (1996). An analysis of Antarctic sea-ice and extratropical cyclone associations. *Int. J. Climatol.*, *16*, 1315–1332. https://doi.org/10.1002/(SICI)1097-0088(199612)16:12<1315::AID-JOC92>3.0.CO;2-M

Hepworth, E., Messori, G., & Vichi, M. (2024). Synoptic-scale extreme variability of winter Antarctic sea-ice concentration and its link to Southern Ocean extratropical cyclones. *J. Geophys. Res.: Oceans*, 129, e2023JC019825. https://doi.org/10.1029/2023JC019825

Hersbach, H., et al. (2020). The ERA5 global reanalysis. *Quart. J. Roy. Meteor. Soc.*, *146*, 1999–2049. https://doi.org/10.1002/qj.3803

Hersbach, H., et al. (2023a). ERA5 hourly data on pressure levels from 1940 to present [Dataset]. Copernicus Climate Change Service (C3S) Climate Data Store (CDS). https://doi.org/10.24381/cds.bd0915c6

Hersbach, H., et al. (2023b). ERA5 hourly data on single levels from 1940 to present [Dataset]. Copernicus Climate Change Service (C3S) Climate Data Store (CDS). https://doi.org/10.24381/cds.adbb2d47

Hirahara, S., Balmaseda, M., Boisseson, E., et al. (2016). Sea surface temperature and sea ice concentration for ERA5. Eur. Centre Medium Range Weather Forecasts, Berkshire, UK, ERA Rep. Ser, 26.

Hobbs, W., Massom, R., Stammerjohn, S., Reid, P., Williams, G., & Meier, W. (2016). A review of recent changes in Southern Ocean sea ice, their drivers and forcings. *Global Planet. Change*, 143, 228–250. https://doi.org/10.1016/j.gloplacha.2016.06.008

Hodges, K. (1994). A general method for tracking analysis and its application to meteorological data. *Mon. Wea. Rev.*, *122*, 2573–2586. https://doi.org/10.1175/1520-0493(1994)122<2573>2.0.CO;2

Hodges, K. (1995). Feature tracking on the unit sphere. *Mon. Wea. Rev.*, 123, 3458–3465. https://doi.org/10.1175/1520-0493(1995)123<3458>2.0.CO;2.

Hodges, K. (1999). Extension of spherical nonparametric estimators to nonisotropic kernels: An oceanographic application. *Mon. Wea. Rev.*, *127*, 214–227. https://doi.org/10.1175/1520-0493(1999)127<0214>2.0.CO;2.

Hoskins, B. J. & Hodges, K. I. (2005). A New Perspective on Southern Hemisphere Storm Tracks. *Journal of Climate*, 18, 4108–4129. https://doi.org/10.1175/JCLI3570.1

Howarth, D. (1983). An analysis of the variability of cyclones around Antarctica and their relationship to sea-ice extent. *Ann. Assoc. Am. Geogr.*, *73*, 519–537. https://doi.org/10.1111/j.1467-8306.1983.tb01856.x

Irving, D., Simmonds, I., & Keay, K. (2010). Mesoscale cyclone activity over the ice-free Southern Ocean: 1999–2008. *J. Climate*, 23, 5404–5420. https://doi.org/10.1175/2010JCLI3628.1

Ionita, M., Scholz, P., Grosfeld, K., & Treffeisen, R. (2018). Moisture transport and Antarctic sea ice: Austral spring 2016 event. *Earth System Dynamics*, 9, 939–954. https://doi.org/10.5194/esd-9-939-2018

Jena, B., Bajish, C., Turner, J., Ravichandran, M., Kshitija, S., Kumar, A., et al. (2022). Mechanisms associated with the rapid decline in sea ice cover around a stranded ship in the Lazarev Sea, Antarctica. *Sci. Total Environ.*, *821*, 153379. https://doi.org/10.1016/j.scitotenv.2022.153379

Jena, B., Bajish, C. C., Turner, J., Ravichandran, M., Kumar, A. N., & Kshitija, S. (2022). Record low sea ice extent in the Weddell Sea, Antarctica in April/May 2019 driven by explosive polar cyclones. *Climate and Atmospheric Science*, *5*, 19. https://doi.org/10.1038/s41612-022-00243-9

Jena, B., Kshitija, S., Bajish, C. C., Turner, J., Holmes, C., Wilkinson, J., Mohan, R., & Thamban, M. (2024). Evolution of Antarctic sea ice ahead of the record low annual maximum extent in September 2023. *Geophys. Res. Lett.*, *51*, e2023GL107561. https://doi.org/10.1029/2023GL107561

Jones, J., Gille, S., Goosse, H., et al. (2016). Assessing recent trends in high-latitude Southern Hemisphere surface climate. *Nature Clim Change*, *6*, 917–926. https://doi.org/10.1038/nclimate3103

Jenkins, M., & Dai, A. (2022). Arctic climate feedbacks in ERA5 reanalysis: Seasonal and spatial variations and the impact of sea-ice loss. *Geophysical Research Letters*, *49*, e2022GL099263. https://doi.org/10.1029/2022GL099263

Maksym, T. (2019). Arctic and Antarctic sea ice change: contrasts, commonalities, and causes. *Annual Review of Marine Science*, *11*, 187–213. https://doi.org/10.1146/annurev-marine-010816-060610

Meehl, G. A., Arblaster, J. M., Chung, C. T. Y., Holland, M. M., DuVivier, A., Thompson, L., Yang, D., & Bitz, C. M. (2019). Sustained ocean changes contributed to sudden Antarctic sea ice retreat in late 2016. *Nature Communication*, *10*, 14. https://doi.org/10.1038/s41467-018-07865-9.

Menéndez, C., Serafini, V., & Le Treut, H. (1999). The effect of sea-ice on the transient atmospheric eddies of the Southern Hemisphere. *Climate Dynamics*, *15*, 659–671. https://doi.org/10.1007/s003820050308

Nghiem, S. V., Rigor, I. G., Clemente-Colón, P., Neumann, G., & Li, P. P. (2016). Geophysical constraints on the Antarctic sea ice cover. *Remote Sensing of Environment*, *181*, 281–292. https://doi.org/10.1016/j.rse.2016.04.005

Parish, T., & Cassano, J. (2003). The role of katabatic winds on the Antarctic surface wind regime. *Mon. Wea. Rev.*, *131*, 317–333. https://doi.org/10.1175/1520-0493(2003)131<0317>2.0.CO;2

Papritz, L., Pfahl, S., Sodemann, H., & Wernli, H. (2015). A climatology of cold air outbreaks and their impact on air–sea heat fluxes in the high-latitude South Pacific. *J. Climate*, *28*, 342–364. https://doi.org/10.1175/JCLI-D-14-00482.1

Parkinson, C., & Cavalieri, D. (2012). Antarctic sea ice variability and trends, 1979-2010. *Cryosphere*, *6*, 871–880. https://doi.org/10.5194/tc-6-871-2012

Parkinson, C., & Comiso, J. (2013). On the 2012 record low Arctic sea ice cover: Combined impact of preconditioning and an August storm. *Geophys. Res. Lett.*, *40*, 1356–1361. https://doi.org/10.1002/grl.50349

Parkinson, C., & DiGirolamo, N. (2016). New visualizations highlight new information on the contrasting Arctic and Antarctic sea-ice trends since the late 1970s. *Remote Sensing of Environment*, *183*, 198–204. https://doi.org/10.1016/j.rse.2016.05.020

Parkinson, C. (2019). A 40-y record reveals gradual Antarctic sea ice increases followed by decreases at rates far exceeding the rates seen in the Arctic. *Proceedings of the National Academy of Sciences*, *116*, 14414–14423. https://doi.org/10.1073/pnas.1906556116

Parkinson, C., & DiGirolamo, N. (2021). Sea ice extents continue to set new records: Arctic, Antarctic, and global results. *Remote Sensing of Environment*, *267*, 112753. https://doi.org/10.1016/j.rse.2021.112753

Perlwitz, J. (2011). Tug of war on the jet stream. *Nature Clim Change*, *1*, 29–31. https://doi.org/10.1038/nclimate1065

Petty, A., Stroeve, J., Holland, P., Boisvert, L., Bliss, A., Kimura, N., & Meier, W. (2018). The Arctic sea ice cover of 2016: a year of record-low highs and higher-than-expected lows. *The Cryosphere*, *12*, 433–452. https://doi.org/10.5194/tc-12-433-2018

Pezza, A., Durrant, T., Simmonds, I., & Smith, I. (2008). Southern Hemisphere synoptic behavior in extreme phases of SAM, ENSO, sea ice extent, and Southern Australia rainfall. *J. Climate*, *21*, 5566–5584. https://doi.org/10.1175/2008JCLI2128.1

Pirti, A., Yucel, M., & Hoşbaş, R. (2012). Displacement of the South Pole from 2006 to 2021: Role of sea ice and Antarctic surface temperature. *Czech Polar Reports*, *12*, 203–221. https://doi.org/10.5817/CPR2022-2-15

Ponce de León, S., & Bettencourt, J. H. (2021). Composite analysis of North Atlantic extra-tropical cyclone waves from satellite altimetry observations. *Adv. Space Res.*, *68*, 762–772, https://doi.org/10.1016/j.asr.2019.07.021

Rudeva, I., & Gulev, S. K. (2011). Composite analysis of North Atlantic extratropical cyclones in NCEP–NCAR reanalysis data. *Mon. Wea. Rev.*, *139*, 1419–1446, https://doi.org/10.1175/2010MWR3294.1

Schemm, S. (2018). Regional trends in weather systems help explain Antarctic sea ice trends. *Geophys. Res. Lett.*, *45*, 7165–7175. https://doi.org/10.1029/2018GL079109

Schroeter, S., O'Kane, T. J., & Sandery, P. A. (2023). Antarctic sea ice regime shift associated with decreasing zonal symmetry in the Southern Annular Mode. *The Cryosphere*, *17*, 701–717. https://doi.org/10.5194/tc-17-701-2023

Serreze, M., & Stroeve, J. (2015). Arctic sea ice trends, variability and implications for seasonal ice forecasting. *Philosophical Transactions of the Royal Society A: Mathematical, Physical and Engineering Sciences*, *373*, 20140159. https://doi.org/10.1098/rsta.2014.0159

Simmonds, I., & Wu, X. (1993). Cyclone behaviour response to changes in winter Southern Hemisphere sea-ice concentration. *Q.J.R. Meteorol. Soc.*, *119*, 1121–1148. https://doi.org/10.1002/qj.49711951313

Simmonds, I. (1996). Climatic role of Southern Hemisphere extratropical cyclones and their relationship with sea ice. *Papers and Proceedings of the Royal Society of Tasmania*, *130*, 95–100. https://doi.org/10.26749/rstpp.130.2.95

Simmonds, I. (2003). Regional and large-scale influences on Antarctic Peninsula climate. In Antarctic Peninsula climate variability: historical and paleoenvironmental perspectives, *79*, 31–42. https://doi.org/10.1029/AR079p0031

Simmonds, I., & Rudeva, I. (2012). The great Arctic cyclone of August 2012. *Geophys. Res. Lett.*, *39*, L23709. https://doi.org/10.1029/2012GL054259

Stammerjohn, S., & Maksym, T. (2017). Gaining (and losing) Antarctic sea ice: variability, trends and mechanisms. In *Sea Ice*, ed. D. N. Thomas, pp. 261–89. Chichester, UK: Wiley & Sons.

Stoll, P. J. (2022). A global climatology of polar lows investigated for local differences and wind-shear environments. *Weather and Climate Dynamics*, *3*, 483–504. https://doi.org/10.5194/wcd-3-483-2022

Streten, N. (1983). Antarctic sea ice and related atmospheric circulation during FGGE. *Arch. Met. Geoph. Biocl. A.*, *32*, 231–246. https://doi.org/10.1007/BF02291894

Stuecker, M. F., Bitz, C. M., & Armour, K. C. (2017). Conditions leading to the unprecedented low Antarctic sea ice extent during the 2016 austral spring season. *Geophys. Res. Lett., 44*, 9008–9019. https://doi.org/10.1002/2017GL075017

Titchner, H., & Rayner, N. (2014). The Met Office Hadley Centre sea ice and sea surface temperature data set, version 2: 1. Sea ice concentrations. *Journal of Geophysical Research: Atmospheres*, *119*, 2864–2889. https://doi.org/10.1002/2013JD020316

Turner, J., Phillips, T., Marshall, G., Hosking, J., Pope, J., Bracegirdle, T., & Deb, P. (2017). Unprecedented springtime retreat of Antarctic sea ice in 2016. *Geophys. Res. Lett. 44*, 6868–6875. https://doi.org/10.1002/2017GL073656

Turner, J., Holmes, C., Caton Harrison, T., Phillips, T., Jena, B., Reeves-Francois, T., et al. (2022). Record Low Antarctic Sea Ice Cover in February 2022. *Geophys. Res. Lett.*, *49*. https://doi.org/10.1029/2022GL098904

Uotila, P., Vihma, T., Pezza, A., Simmonds, I., Keay, K., & Lynch, A. (2011). Relationships between Antarctic cyclones and surface conditions as derived from high-resolution numerical weather prediction data. *J. Geophys. Res.*, *116*, D07109. https://doi.org/10.1029/2010JD015358

Vichi, M., Eayrs, C., Alberello, A., Bekker, A., Bennetts, L., Holland, D., et al. (2019). Effects of an explosive polar cyclone crossing the Antarctic marginal ice zone. *Geophys. Res. Lett.*, *46*, 5948–5958. https://doi.org/10.1029/2019gl082457

Vihma, T. (2014). Effects of Arctic Sea Ice Decline on Weather and Climate: A Review. *Surv Geophys*, *35*, 1175–1214. https://doi.org/10.1007/s10712-014-9284-0

Wang, Z., Turner, J., Sun, B., Li, B., & Liu, C. (2014). Cyclone-induced rapid creation of extreme Antarctic sea ice conditions. *Sci. Rep.*, *4*, 5317. https://doi.org/10.1038/srep05317

Wang, X., Zhang, Z., Wang, X., Vihma, T., Zhou, M., Yu, L., Uotila, P., & Sein, D. (2021). Impacts of strong wind events on sea ice and water mass properties in Antarctic coastal polynyas. *Clim. Dyn.*, *57*, 3505–3528. https://doi.org/10.1007/s00382-021-05878-7

Wang, J., Luo, H., Yang, Q., Liu, J., Yu, L., Shi, Q., & Han, B. (2022). An Unprecedented Record Low Antarctic Sea-ice Extent during Austral Summer 2022. *Advances in Atmospheric Sciences*, *39*, 1591–1597. https://doi.org/10.1007/s00376-022-2087-1

Wang, X., Zhang, Z., Dinniman, M., Uotila, P., Li, X., & Zhou, M. (2023). The response of sea ice and high-salinity shelf water in the Ross Ice Shelf Polynya to cyclonic atmosphere circulations. *The Cryosphere*, *17*, 1107–1126. https://doi.org/10.5194/tc-17-1107-2023

Ward, J. L., Payne, A. E., & Pettersen, C. (2023). Present-day regional Antarctic Sea Ice response to extratropical cyclones. *Journal of Geophysical Research: Atmospheres*, *128*, e2023JD038914. https://doi.org/10.1029/2023JD038914

Watkins, A. B., & Simmonds, I. (1995). Sensitivity of numerical prognoses to Antarctic sea ice distribution. *J. Geophys. Res.*, *100*, 22681–22696. https://doi.org/10.1029/95JC02581

Watkins, A., & Simmonds, I. (1998). Relationships between Antarctic sea-ice concentration, wind stress and temperature temporal variability, and their changes with distance from the coast. *Annals of Glaciology*, *27*, 409–412. https://doi.org/10.3189/1998AoG27-1-409-412

Yuan, X., Martinson, D., & Liu, W. (1999). Effect of air-sea-ice interaction on winter 1996 Southern Ocean subpolar storm distribution. *J. Geophys. Res.*, *104*, 1991–2007. https://doi.org/10.1029/98JD02719

Zhang, J., Lindsay, R., Schweiger, A., & Steele, M. (2013). The impact of an intense summer cyclone on 2012 Arctic sea ice retreat. *Geophys. Res. Lett.*, *40*, 720–726. https://doi.org/10.1002/grl.50190

Zhang, L., Ren, X., Wang, C. Y., et al. (2024). An observational study on the interactions between storm tracks and sea ice in the Southern Hemisphere. *Clim. Dyn.*, *62*, 17–36. https://doi.org/10.1007/s00382-023-06894-5

Zhong, R., Yang, Q., Hodges, K., Wu, R., & Chen, D. (2022). Impact of Data Resolution on Tracking Southern Ocean Cyclones. *Mon. Wea. Rev.*, *151*, 3–22. https://doi.org/10.1175/MWR-D-22-0121.1

Zwally, H., Comiso, J., Parkinson, C., Cavalieri, D., & Gloersen, P. (2002). Variability of Antarctic sea ice 1979-1998. *J. Geophys. Res.*, *107*, 3041. https://doi.org/10.1029/2000JC000733